

Dynamical gluon effects in twist-3 generalized parton distributions of the proton

Ziqi Zhang,^{1, 2, 3, *} Chandan Mondal,^{1, 2, 3, †} Sisi Xu,^{1, 2, 3, ‡} Xingbo Zhao,^{1, 2, 3, §} and James P. Vary^{4, ¶}
(BLFQ Collaboration)

¹*Institute of Modern Physics, Chinese Academy of Sciences, Lanzhou 730000, China*

²*School of Nuclear Science and Technology, University of Chinese Academy of Sciences, Beijing 100049, China*

³*CAS Key Laboratory of High Precision Nuclear Spectroscopy,*

Institute of Modern Physics, Chinese Academy of Sciences, Lanzhou 730000, China

⁴*Department of Physics and Astronomy, Iowa State University, Ames, IA 50011, U.S.A.*

(Dated: January 13, 2026)

Within the Basis Light-Front Quantization framework, we systematically investigate the subleading-twist (twist-3) generalized parton distributions (GPDs) of the proton's valence quarks beyond the Wandzura–Wilczek (WW) approximation. The twist-3 GPDs are not independent; through the equations of motion they decompose into a non-genuine contribution and a genuine twist-3 term. The latter encodes quark–gluon–quark correlations and involves interference between the light-front Fock sectors $|qqq\rangle$ and $|qqgg\rangle$, which are typically neglected in the WW approximation. Using light-front wave functions obtained from diagonalizing the proton light-front Hamiltonian for its $|qqq\rangle$ and $|qqgg\rangle$ Fock components, we compute these GPDs via their overlap representations. To further explore their physical implications, we also evaluate several twist-3-related quantities, including the quark orbital angular momentum, the total quark spin contribution, and the quark spin–orbit correlation. Our results provide new nonperturbative input on higher-twist dynamics particularly multi-parton interference effects relevant for future measurements at the EicC and the EIC.

I. INTRODUCTION

One of the most intriguing problems in modern physics is the exploration of the proton's internal structure and its spin puzzle, both experimentally and theoretically (see Refs. [1, 2] and references therein). A powerful tool for probing the proton structure is deeply virtual Compton scattering (DVCS), in which a quark absorbs a virtual photon emitted by an electron, promptly emits a real photon, and then returns to the proton. This process has been measured in numerous experiments, including JLab CLAS [3–6], JLab Hall A [7, 8], HERA H1 [9–11], HERA ZEUS [9, 12], and HERA HERMES [13, 14]. Further measurements are anticipated at the future Electron–Ion Collider (EIC) [15] and the Electron–Ion Collider in China (EicC) [16].

A variety of distribution functions describe the proton's internal structure at the partonic level. For hard exclusive processes (e.g., DVCS), generalized parton distributions (GPDs) are employed, providing access to the proton's three-dimensional structure. GPDs have attracted significant interest because they are related to conventional observables while encoding much richer information. In the forward limit ($\Delta \rightarrow 0$), one recovers the ordinary parton distribution functions (PDFs), which describe the longitudinal momentum distributions of quarks and gluons in the proton. Conversely, in-

tegrating GPDs over the longitudinal momentum fraction yields the electromagnetic form factors (FFs), which characterize the proton's charge and magnetization distributions.

Several theoretical studies of proton GPDs have been carried out using a wide range of QCD-inspired models, including the bag model [17, 18], soliton models [19–21], constituent quark models (CQMs) [22–26], light-front (LF) quark–diquark models [27–31], meson-cloud models [32, 33], and approaches based on AdS/QCD [34–39]. Additional progress has been made within LF quantization frameworks [40–45]. At the same time, Euclidean lattice QCD has emerged as a promising first-principles framework for computing GPDs [46–57].

However, most of the studies mentioned above focus on the leading-twist (twist-2) level. Twist-3 distributions are often assumed to be small because they are suppressed by a factor of $1/Q$, where Q denotes the four-momentum transfer of the process. In reality, twist-3 effects are non-negligible and play an important role in revealing the proton's internal structure [45, 58, 59]. First, twist-3 distributions are directly connected to quark orbital angular momentum (OAM) and quark spin–orbit correlations [60–62]. Second, they are related to the average transverse color Lorentz force experienced by quarks [63, 64]. Third, twist-3 GPDs at nonzero skewness enter the twist-3 DVCS amplitude through the corresponding Compton form factors (CFFs) [65].

In this work, we employ the theoretical framework of Basis Light-Front Quantization (BLFQ) [66] and use light-front wave functions (LFWFs), obtained by diagonalizing the LFQCD Hamiltonian, to calculate all twist-3 GPDs in the zero-skewness limit. In contrast to previous studies [45], our approach extends the Fock-

* zhangziqi@impcas.ac.cn

† mondal@impcas.ac.cn

‡ xsq234@impcas.ac.cn

§ xbzhao@impcas.ac.cn

¶ jvary@iastate.edu

space truncation to include the first two sectors, $|qqq\rangle$ and $|qqqg\rangle$, thereby incorporating contributions from quark–gluon–quark correlations. This goes beyond the Wandzura–Wilczek (WW) approximation [67–70]. We further explore the connections between twist-3 GPDs, quark OAM, and quark spin–orbit correlations.

The structure of this work is as follows: Sec. II provides a brief introduction to the BLFQ framework; Sec. III outlines GPDs and presents the twist decomposition of GPDs; Sec. IV reports numerical results for twist-3 zero-skewness GPDs within the first two Fock sectors, along with their properties in the forward limit; Sec. V summarizes the work and discusses future prospects.

II. BASIS LIGHT-FRONT QUANTIZATION

As a non-perturbative approach, BLFQ is grounded in the Hamiltonian formalism and leverages the advantages of LF dynamics. Its core idea is to simultaneously obtain the mass spectrum and bound state wavefunctions by solving the eigenvalue problem

$$P^- P^+ |\psi\rangle = M^2 |\psi\rangle, \quad (1)$$

where P^+ and P^- denote the longitudinal momentum and the LF Hamiltonian of the system, respectively, with the ‘ \pm ’ components being defined as $P^\pm = P^0 \pm P^3$. Here, M^2 is the eigenvalue corresponding to the LF energy of the system, and the eigenvector $|\psi\rangle$, representing the proton state, is expanded as

$$|\psi_{\text{proton}}\rangle = \Phi^{qqq} |qqq\rangle + \Phi^{qqqg} |qqqg\rangle + \dots, \quad (2)$$

where Φ are the corresponding LFWFs, and the ‘ \dots ’ represents all other possible partonic combinations that can be found inside the proton.

At the initial scale, where the proton state is described by the $|qqq\rangle$ and $|qqqg\rangle$ Fock components, we employ the LF Hamiltonian $P^- = P_{\text{QCD}}^- + P_{\text{C}}^-$, where P_{QCD}^- incorporates the relevant QCD interactions and P_{C}^- models confinement [71]. In the LF gauge $A^+ = 0$, the LF QCD Hamiltonian with one dynamical gluon is given by [71]

$$P_{\text{QCD}}^- = \int d^2 x^\perp dx^- \left\{ \frac{1}{2} \bar{\psi} \gamma^+ \frac{m_0^2 + (i\partial^\perp)^2}{i\partial^+} \psi \right. \\ \left. + \frac{1}{2} A_a^i [m_g^2 + (i\partial^\perp)^2] A_a^i + g_s \bar{\psi} \gamma_\mu T^a A_a^\mu \psi \right. \\ \left. + \frac{1}{2} g_s^2 \bar{\psi} \gamma^+ T^a \psi \frac{1}{(i\partial^+)^2} \bar{\psi} \gamma^+ T^a \psi \right\}, \quad (3)$$

where the first and second terms ¹ account for the kinetic energies of the quark (with bare mass m_0) and gluon (with bare mass m_g), respectively, while the last

two terms represent the vertex and instantaneous interactions, characterized by the strong coupling g_s . A detailed description and physical interpretation of these terms can be found in Refs. [71–73].

Confinement in the leading Fock sector is implemented following Ref. [74] as

$$P_{\text{C}}^- P^+ = \frac{\kappa^4}{2} \sum_{i \neq j} \left[\vec{r}_{ij\perp}^2 - \frac{\partial_{x_i} (x_i x_j \partial_{x_j})}{(m_i + m_j)^2} \right], \quad (4)$$

where $\vec{r}_{ij\perp} = \sqrt{x_i x_j} (\vec{r}_{i\perp} - \vec{r}_{j\perp})$ denotes the transverse separation between quarks i and j , while κ is the confinement strength. In the $|qqqg\rangle$ sector, we omit an explicit confinement term, assuming that the restricted transverse basis together with the inclusion of a massive gluon effectively captures the essential confinement behavior.

The many-particle basis includes the transverse center-of-mass (CM) motion that is entangled with the intrinsic motion. Consequently, it is essential to introduce a constraint term [66] into the effective Hamiltonian

$$H' = \lambda_L (H_{\text{cm}} - 2b^2 I), \quad (5)$$

where λ_L denotes the Lagrange multiplier, $2b^2$ represents the zero-point energy, and I is the identity operator. By choosing a sufficiently large λ_L , one can shift the excited states of the CM motion to higher energies and ensure that all low-lying states correspond to the ground state of the CM motion.

We solve the LF Hamiltonian eigenvalue problem within the BLFQ framework [66], expanding the proton in a basis of longitudinal plane waves (in a box of length $2L$ with antiperiodic/periodic boundary conditions for quarks/gluons), transverse two-dimensional harmonic oscillator (2D-HO) functions $\Phi_{nm}(\vec{p}_\perp; b)$ [75], and light-cone helicity spinors. Single-particle states are labeled by $\bar{\alpha} = \{k, n, m, \lambda\}$, with k being the longitudinal quantum number (half-integer for quarks, integer for gluons, excluding zero mode); (n, m) are the 2D-HO quantum numbers, and λ the helicity; states in sectors with multiple color-singlets such as $|qqqg\rangle$ require an additional label to distinguish their color singlet configuration.

The basis is truncated by N_{max} and $K = \sum_i k_i$ with the sum running over all i -partons from 1 to N , N_{max} imposes $\sum_i (2n_i + |m_i| + 1) \leq N_{\text{max}}$, while K fixes the longitudinal resolution, with $x_i = k_i/K$. These parameters set the IR/UV scales [75]. Diagonalization yields the proton LFWFs with helicity Λ ,

$$\Psi_{\{x_i, \vec{p}_\perp, \lambda_i\}}^{N, \Lambda} = \sum_{\{n_i, m_i\}} \psi^N(\{\alpha_i\}) \prod_{i=1}^N \Phi_{n_i m_i}(\vec{p}_{i\perp}, b), \quad (6)$$

where $\psi^{N=3}$ and $\psi^{N=4}$ are the eigenvector components for the $|uud\rangle$ and $|uudg\rangle$ sectors.

The Hamiltonian parameters, summarized in Table I with $\{N_{\text{max}}, K\} = \{9, 16.5\}$, are set to reproduce the proton mass and its electromagnetic properties [71]. At the model scale, the proton contains approximately 44%

¹ The sign of the second term of Eq. (2) in Ref. [71] should be +.

probability in the $|qqq\rangle$ sector and 56% in the $|qqqg\rangle$ sector. The resulting LFWFs, appropriate for a low-resolution scale of $\mu_0^2 \sim 0.24 \pm 0.01$ GeV² [71], have been successfully used to describe a broad range of proton observables, including electromagnetic form factors, radii, PDFs, GPDs, TMDs, and spin and orbital angular momentum [43, 44, 71–73, 76, 77].

Table I: Summary of the model parameters [71]. All parameters have units of GeV except for g_s .

m_u	m_d	m_g	κ	m_f	g_s	b	b_{inst}
0.31	0.25	0.50	0.54	1.80	2.40	0.70	3.00

III. GENERALIZED PARTON DISTRIBUTION

In this section, we briefly introduce the definition of twist-3 GPDs. One of the most common definitions is formulated via a bilocal quark-quark correlator, which depends on three variables: x , ξ , and $-t$. Here, x denotes the longitudinal momentum fraction, ξ represents the skewness, and $-t$ stands for the squared momentum transfer. The correlator takes the form

$$F_{\Lambda'\Lambda}^{[\Gamma]}(x, \xi, -t) = \frac{1}{2} \int \frac{dy^-}{4\pi} e^{ixP\cdot y} \left\langle P', \Lambda' \left| \bar{\Psi} \left(-\frac{y}{2} \right) \right. \right. \\ \times \mathcal{W} \left(-\frac{y}{2}, \frac{y}{2} \right) \Gamma \Psi \left(\frac{y}{2} \right) \left. \left| P, \Lambda \right\rangle \right|_{y^+=0, \vec{y}^\perp=0}, \quad (7)$$

where $|P, \Lambda\rangle$ describes the momentum and helicity of the initial proton state, while the primed bra vector ($\langle P', \Lambda'|$) corresponds to the final proton state. The Wilson line is defined as $\mathcal{W}(y_2, y_1) \equiv P \exp(i g_s \int_{y_1}^{y_2} dz^\mu A_\mu(z))$; under the light-cone gauge ($A^+ = 0$), this Wilson line reduces to unity. Γ denotes one of the complete set of Dirac matrices, and $\Psi(x)$ represents the quark field. As we will see, not all components of $\Psi(x)$ are independent dynamical degrees of freedom.

By applying a projection operator \mathcal{P}^\pm , the quark field can be decomposed into dynamical and non-dynamical components [78], i.e., $\Psi = \Psi^+ + \Psi^-$. Here, $\Psi^\pm = \mathcal{P}^\pm \Psi$ with $\mathcal{P}^\pm = \gamma^\mp \gamma^\pm / 4$. The dynamical component Ψ^+ is expanded in the form of a free fermion field, while the non-dynamical component Ψ^- is constrained by the Dirac equation,

$$\Psi^- = \frac{\gamma^+}{2i\partial^+} (m_q - i\gamma^\perp \partial_\perp + g_s \gamma^\perp A_\perp) \Psi^+, \quad (8)$$

where m_q is the quark mass, g_s is the coupling constant, and A_μ is the gluon field. Herein, summation over all repeated indices is implied by default.

For the DVCS process ($ep \rightarrow e'p'\gamma$) associated with GPDs, we adopt a symmetric frame for the initial and final proton momenta. In this frame, the four-momenta

of the incoming and outgoing protons are given by

$$P = \left((1 + \xi) \bar{P}^+, -\frac{\vec{\Delta}^\perp}{2}, \frac{M^2 + (\vec{\Delta}^\perp)^2/4}{(1 + \xi) \bar{P}^+} \right), \quad (9)$$

$$P' = \left((1 - \xi) \bar{P}^+, \frac{\vec{\Delta}^\perp}{2}, \frac{M^2 + (\vec{\Delta}^\perp)^2/4}{(1 - \xi) \bar{P}^+} \right), \quad (10)$$

$$\Delta = P' - P = \left(-2\xi \bar{P}^+, \vec{\Delta}^\perp, \frac{t - (\vec{\Delta}^\perp)^2}{2\xi \bar{P}^+} \right), \quad (11)$$

where $\bar{P} = (P + P')/2$ is the average momentum of the proton, Δ is the momentum transfer, $\xi = -\Delta^+/(2\bar{P}^+)$ is the skewness, M is the proton mass, and $t \equiv -\Delta^2$ is the squared momentum transfer.

Based on the definitions of twist and Dirac matrices, the physical observables for the twist-3 case correspond to the interference terms $\bar{\Psi}^+ \Gamma \Psi^-$ and $\bar{\Psi}^- \Gamma \Psi^+$. By contrast, the twist-2 case is characterized by $\bar{\Psi}^+ \Gamma \Psi^+$, and the twist-4 case by $\bar{\Psi}^- \Gamma \Psi^-$. Using this general expression, the GPDs can be computed through the parametrization of Ref. [79]. Several parametrization schemes for GPDs have been developed [80–85], among which the scheme of Ref. [86] is the most extensively studied and is directly related to the present work [80] (see Appendix B). The full overlap expressions for all twist-3 GPDs are provided in Appendix A. For the corresponding overlap formulas truncated to the lowest Fock sector, we refer the reader to our earlier study [45].

IV. NUMERICAL RESULTS AND DISCUSSION

In this section, we present numerical results for zero-skewness twist-3 GPDs calculated via the BLFQ method. The key distinction between this work and previous studies [45] lies in the inclusion of two Fock sectors, $|qqq\rangle + |qqqg\rangle$, which incorporates gluon contributions—specifically, the $q\text{-}g\text{-}q$ interaction. We further analyze the properties of these twist-3 GPDs, including sum rules, spin-orbit correlations, and OAM. Note that properties such as time-reversal symmetry have been discussed in prior work and are not revisited herein.

The inclusion of two Fock sectors substantially increases the complexity of the overlap representation, primarily due to the emergence of the $q\text{-}g\text{-}q$ correlator. Each twist-3 GPD consists of three distinct components: the qqq component, which arises from the overlap between the states $\langle qqq|$ and $|qqq\rangle$; the $qqqg$ component, which originates from the overlap between $\langle qqqg|$ and $|qqqg\rangle$; and the “genuine” (abbreviated as “gen”) component, which accounts for cross-overlap contributions, i.e., between $\langle qqq|$ and $|qqqg\rangle$, and between $\langle qqqg|$ and $|qqq\rangle$.

A. Twist-3 GPDs

For all results presented here, the rotational symmetry between γ_1 and γ_2 is preserved—not only for each indi-

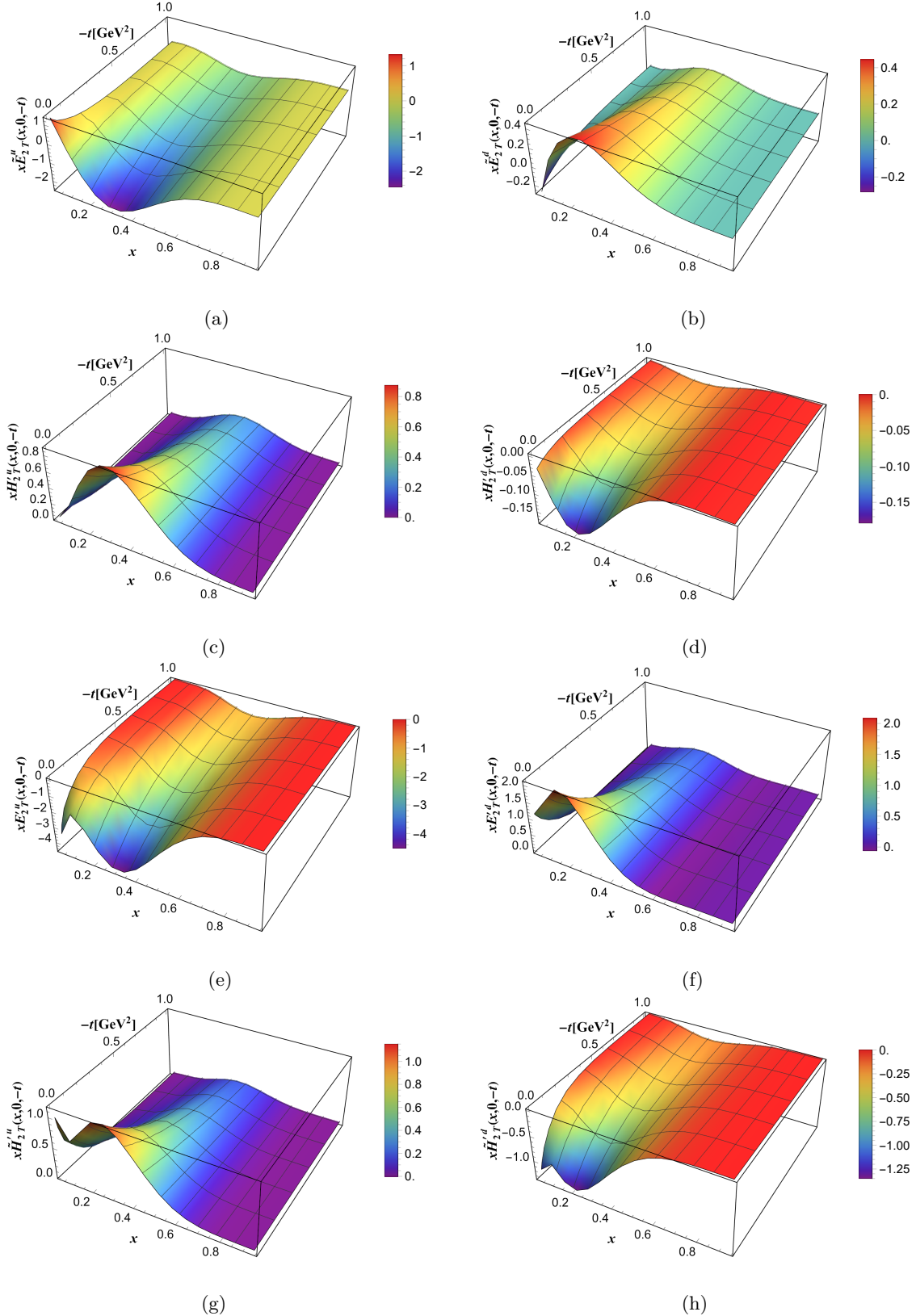


Figure 1: 3D Plots of the twist-3 quark GPDs $x\tilde{E}_{2T}$, xH'_{2T} , xE'_{2T} , and $x\tilde{H}'_{2T}$ in the proton, evaluated with $N_{\max} = 9$ and $K = 16.5$. The left column panels {(a), (c), (e), (g)} correspond to the u quark and the right column panels {(b), (d), (f), (h)} correspond to the d quark on the flavor level. The flavor level distributions are given by $X_{\text{flavor}}^u = 2X_{\text{quark}}^u$ and $X_{\text{flavor}}^d = X_{\text{quark}}^d$, where X stands for all the GPDs.

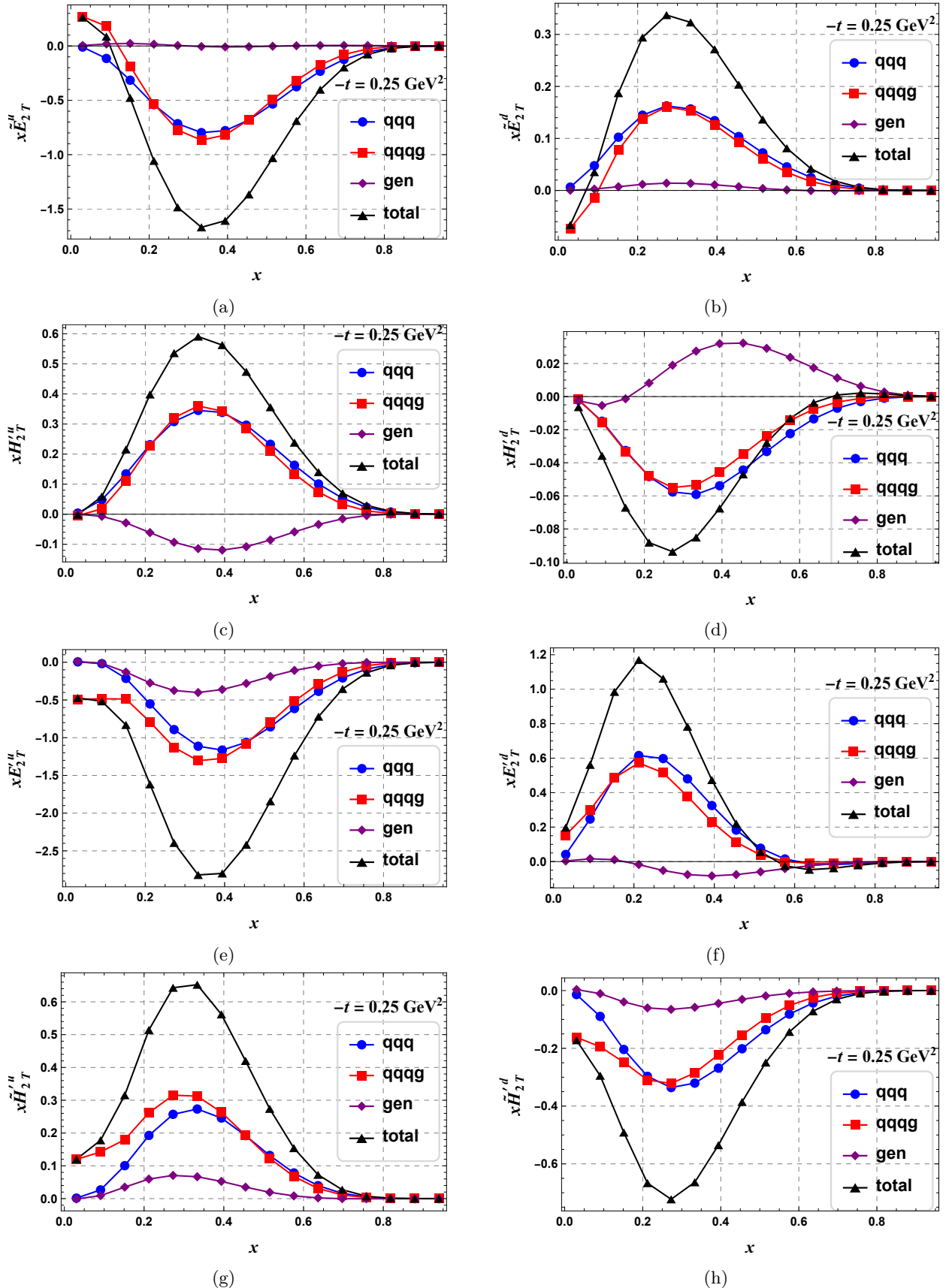


Figure 2: 2D Plots of the twist-3 quark GPDs $x\tilde{E}_{2T}$, xH'_{2T} , xE'_{2T} , and $x\tilde{H}'_{2T}$ in the proton at fixed $-t = 0.25 \text{ GeV}^2$, evaluated with $N_{\max} = 9$ and $K = 16.5$. The left column panels $\{(a), (c), (e), (g)\}$ correspond to the u quark and the right column panels $\{(b), (d), (f), (h)\}$ correspond to the d quark on the flavor level. The flavor level distributions are given by $X_{flavor}^u = 2X_{quark}^u$ and $X_{flavor}^d = X_{quark}^d$, where X stands for all the GPDs.

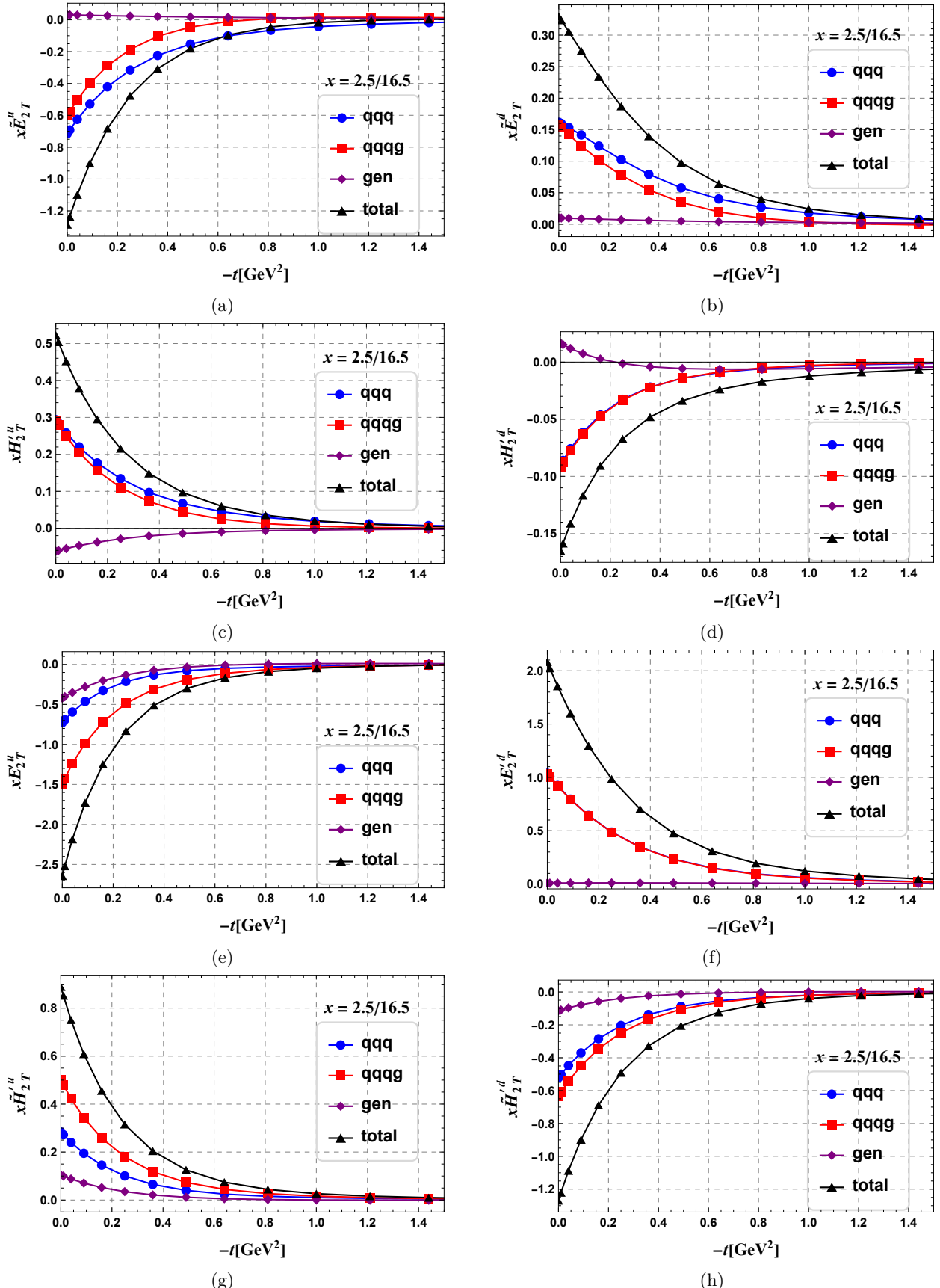


Figure 3: 2D Plots of the twist-3 quark GPDs $x\tilde{E}_{2T}$, xH'_{2T} , xE'_{2T} , and $x\tilde{H}'_{2T}$ in the proton at fixed $x = 2.5/16.5$, evaluated with $N_{\max} = 9$ and $K = 16.5$. The left column panels {(a), (c), (e), (g)} correspond to the u quark and the right column panels {(b), (d), (f), (h)} correspond to the d quark on the flavor level. The flavor level distributions are given by $X_{\text{flavor}}^u = 2X_{\text{quark}}^u$ and $X_{\text{flavor}}^d = X_{\text{quark}}^d$, where X stands for all the GPDs.

vidual component but also for their sum. For simplicity, γ_1 is used for calculations. Given that $\xi = 0$ is fixed in this work, the GPDs are presented as functions of x and $-t$. In the zero-skewness limit, eight of the twist-3 GPDs— H_{2T} , E_{2T} , \tilde{H}_{2T} , \tilde{E}'_{2T} , \tilde{H}_2 , H'_2 , E'_2 , and \tilde{E}'_2 —are found to be consistent with zero within our numerical uncertainty.

Using the overlap representation and the LFWFs obtained by solving the BLFQ framework, we calculate all the twist-3 GPDs. For brevity, we present only the four most extensively studied chiral-even GPDs: these are parameterized from the vector current (γ^\perp) and pseudo-vector current ($\gamma^\perp \gamma_5$), namely \tilde{E}_{2T} (from vector current) and H'_{2T} , E'_{2T} , H'_{2T} (from pseudo-vector current). These GPDs have been shown to relate to G_i and G'_i (where $i = 1, 4$) [80]. Each two-dimensional subplot distinguishes contributions from the qqq sector (blue solid circles), $qqqg$ sector (red solid squares), genuine (gen) contribution (purple solid diamonds), and total GPD (black solid triangles); since the magnitudes of these curves are excessively large, we multiply by x to suppress their values.

In Fig. 1, we present the three-dimensional structure of the twist-3 GPDs in the zero-skewness limit. The results are plotted up to $-t = 1.0 \text{ GeV}^2$, which focuses on the region with meaningful structural features. Beyond the upper limit of the depicted range, the magnitude maintains the depicted trends. That is, for $-t > 1.0 \text{ GeV}^2$ (not shown in the figures), the relevant quantities exhibit a featureless falloff to zero.

For $x\tilde{E}_{2T}$, the region of small x and small $-t$ shows a modest peak with a sign opposite to that in the rest of the kinematic domain; moreover, the u and d quark contributions carry opposite signs throughout the full region. In the case of xH'_{2T} , the distribution is smooth across all kinematics. This behavior arises because its overlap representation does not contain Δ in the denominator, a feature that also makes it the only GPD that remains finite in the $\Delta \rightarrow 0$ limit (corresponding to the twist-3 parton distribution function $g_T(x)$).

For xE'_{2T} and $x\tilde{H}'_{2T}$, the two distributions exhibit similar shapes but opposite signs—both between u and d quarks and between the two GPDs for a given quark flavor. Both GPDs also display fluctuations in the small x and small $-t$ region, with signs consistent with their behavior in the rest of the domain. The peak observed at small x and small $-t$ for all of the above GPDs originate from the inclusion of the nonvalence Fock sector with a dynamical gluon. Furthermore, owing to discretization and truncation effects in the longitudinal direction, we are not able to obtain reliable distributions at even smaller values of x .

In Fig. 2, we fix $-t = 0.25 \text{ GeV}^2$ and plot the four GPDs as functions of x . All GPDs show the same trend, with one prominent peak. The gen contribution is much smaller than the other components but remains non-negligible. Most GPDs fluctuate in the small x region: the $qqqg$ sector contribution is particularly notable here,

dominating in the small x region and nearly equal to the total GPD (except for H'_{2T}). This behavior can be attributed to their overlap expressions, where division by Δ amplifies contributions at small $-t$. For the remaining x range, the qqq and $qqqg$ sector contributions are nearly equal, while the gen contribution is minimal. The peaks of all GPDs cluster in the range $0.2 < x < 0.4$, and all tend to zero in the large x regime.

In Fig. 3, we fix $x = 2.5/16.5$ and plot the four GPDs as functions of $-t$. In subplots (a) and (b), the qqq sector contribution is slightly larger than that of the $qqqg$ sector, while the gen contribution remains small. In subplots (c) and (d), the qqq and $qqqg$ sector contributions are comparable. In subplot (e), the $qqqg$ sector contribution is nearly twice that of the qqq sector, while in subplot (f), the two are nearly equal. In subplots (g) and (h), the $qqqg$ sector contribution is larger than that of the qqq sector. All curves show a decreasing trend as $-t$ increases.

B. Spin-orbit correlation

The parity-odd partner of the quark energy-momentum tensor operator, $\hat{T}_{q5}^{\mu\nu}$, is closely related to quark spin-orbit correlations and has been investigated in Ref. [87]. This operator is defined as

$$\hat{T}_{q5}^{\mu\nu} = \frac{1}{2} \bar{\psi} \gamma^\mu \gamma_5 i \overleftrightarrow{D}^\nu \psi, \quad (12)$$

where $\overleftrightarrow{D}^\nu = \overrightarrow{D}^\nu - \overleftarrow{D}^\nu$ denotes the symmetric covariant derivative (with $D^\nu = \partial^\nu - igA^\nu$ as the covariant derivative). To characterize the matrix elements of $\hat{T}_{q5}^{\mu\nu}$ in nucleon states, it is parametrized in terms of five FFs

$$\langle p', s' | \hat{T}_{q5}^{\mu\nu} | p, s \rangle = \bar{u}(p', s') \Gamma_{q5}^{\mu\nu} u(p, s), \quad (13)$$

with

$$\begin{aligned} \Gamma_{q5}^{\mu\nu} = & \frac{P^{\{\mu} \gamma^{\nu\}} \gamma_5}{2} \tilde{A}_q(-t) + \frac{P^{\{\mu} \Delta^{\nu\}} \gamma_5}{4M} \tilde{B}_q(-t) \\ & + \frac{P^{\{\mu} \gamma^{\nu\}} \gamma_5}{2} \tilde{C}_q(-t) + \frac{P^{\{\mu} \Delta^{\nu\}} \gamma_5}{4M} \tilde{D}_q(-t) \\ & + M i \sigma^{\mu\nu} \gamma_5 \tilde{F}_q(-t). \end{aligned} \quad (14)$$

The FFs $\tilde{A}_q(-t)$ and $\tilde{B}_q(-t)$ are associated with the twist-2 contribution obtained by selecting the $\mu\nu = ++$ component of the energy-momentum tensor. In this case, one finds:

$$\int dx x \tilde{H}_q(x, \xi, -t) = \tilde{A}_q(-t), \quad (15)$$

$$\int dx x \tilde{E}_q(x, \xi, -t) = \tilde{B}_q(-t). \quad (16)$$

Taking the twist-3 component $\mu\nu = j+$ with $j = 1, 2$, the following relations are obtained [87]

$$\int dx x \tilde{G}_1^q(x, \xi, -t) = -\frac{1}{2} \left(\tilde{B}_q(-t) + \tilde{D}_q(-t) \right), \quad (17)$$

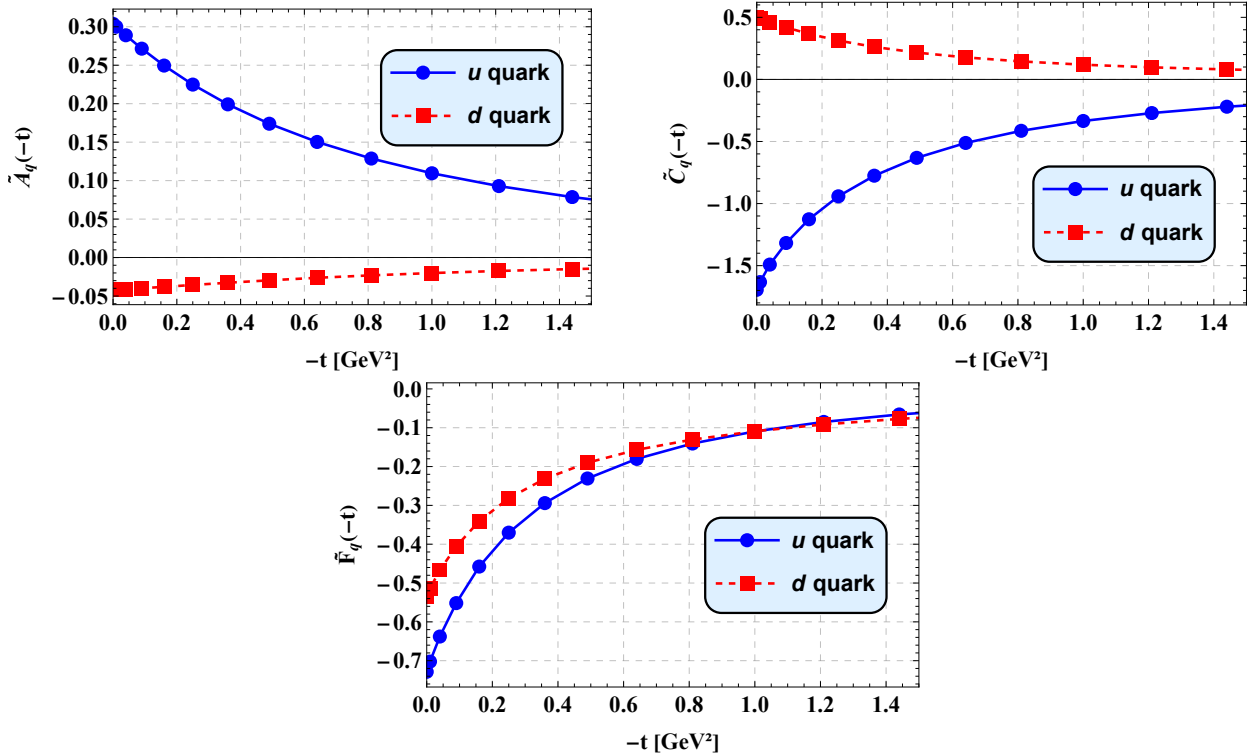


Figure 4: Plots of the twist-3 FFs \tilde{A}_q , \tilde{C}_q and \tilde{F}_q in the proton, evaluated with $N_{\max} = 9$ and $K = 16.5$. The blue circle solid line corresponds to the u quark and the red square dotted line corresponds to the d quark on the quark level.

$$\int dx x \tilde{G}_2^q(x, \xi, -t) = -\frac{1}{2} \left(\tilde{A}_q(-t) + \tilde{C}_q(-t) \right) + (1 - \xi^2) \tilde{F}_q(-t), \quad (18)$$

$$\int dx x \tilde{G}_3^q(x, \xi, -t) = -\frac{\xi}{2} \tilde{F}_q(-t), \quad (19)$$

$$\int dx x \tilde{G}_4^q(x, \xi, -t) = -\frac{1}{2} \tilde{F}_q(-t), \quad (20)$$

where \tilde{G}_i are related to H'_{2T} , E'_{2T} , \tilde{H}'_{2T} , and \tilde{E}'_{2T} [45, 80] (see Appendix. B).

We present the FFs $\tilde{A}_q(-t)$, $\tilde{C}_q(-t)$, and $\tilde{F}_q(-t)$ in Fig. 4. We observe that $\tilde{A}_q(-t)$ and $\tilde{C}_q(-t)$ exhibit similar shapes but have opposite signs—both between u - and d -quarks and between the two form factors for a given quark flavor. Moreover, the u -quark contribution is significantly larger than that of the d -quark. In contrast, $\tilde{F}_q(-t)$ is negative for both flavors and displays a similar overall behavior.

Since we focus on extracting the GPDs at $\xi = 0$, the distributions \tilde{E} and \tilde{G}_1 lie beyond the scope of this work. Consequently, the corresponding form factors $\tilde{B}_q(-t)$ and $\tilde{D}_q(-t)$ are not determined in the present analysis. For clarity, these form factors could, in principle, be obtained by performing calculations at nonzero ξ , where their contributions can be isolated through the full GPD parametrization.

Several well-established relations involving twist-3

GPDs in the forward limit are worth highlighting. The quark OAM in the nucleon is defined, in the limit $\Delta \rightarrow 0$, as [86]

$$L_z^q = -\lim_{\Delta \rightarrow 0} \int dx x G_2^q(x, 0, \Delta_\perp^2), \quad (21)$$

where the explicit expression for G_2^q is provided in Appendix B. This physical quantity can also be calculated directly from twist-2 GPDs, as defined in Refs. [60–62]. Within our BLFQ approach at the model scale, we obtain $L_z^u = 0.107$ ($L_z^d = 0.0752$) from twist-3 distributions and $L_z^u = 0.0817$ ($L_z^d = 0.0264$) from twist-2 GPDs. This difference may arise from the violation of the Burkhardt-Cottingham sum rule [88] ($\int dx g_1(x) = \int dx g_T(x)$) in our results. A similar deviation has also been reported in Ref. [58].

The total quark spin contribution J_z^q can also be related to twist-3 GPDs via [81]

$$J_z^q = \int dx \left(x G_{q,3}(x, 0, 0) - \frac{1}{2} g_1^q(x) \right), \quad (22)$$

where g_1^q is the twist-2 helicity PDF, and $G_{q,3}$ (defined in Ref. [81]) can be converted to $G_{q,3} = -E_{2T}^q$. Using this relation, at the model scale, we find $J_z^u = 0.443$ ($J_z^d = -0.0801$) from twist-3 distributions and $J_z^u = 0.468$ ($J_z^d = -0.0312$) from twist-2 distributions.

For the quark spin-orbit correlation, it is expressed as [87]

$$C_z^q = - \int dx x (\tilde{G}_2^q(x, 0, 0) + 2\tilde{G}_4^q(x, 0, 0)). \quad (23)$$

We list our results in Table II for comparison with other theoretical approaches, including the naive quark model (NQM), the light-front constituent quark model (LFCQM), and the light-front chiral quark-soliton model (LF χ QSM) [89], the Leader-Sidorov-Stamenov (LSS) analysis [90], and the spectator diquark model [58]. The negative signs of the results indicate that the quark spin and Ji OAM are anti-correlated on average [87].

Table II: Comparison of C_z^u and C_z^d values from different theoretical approaches.

Theoretical Approach	C_z^u	C_z^d
BLFQ (model scale, this work)	-0.761	-0.515
NQM, LFCQM, LF χ QSM [89]	≈ -0.8	≈ -0.55
LSS ($\mu^2 = 1$ GeV 2) [90]	≈ -0.9	≈ -0.53
Spectator Diquark Model [58]	-0.775	-0.586

V. CONCLUSION

In this work, we have computed all twist-3 GPDs of the proton in the zero-skewness limit within the BLFQ framework, presenting the four non-vanishing chiral-even distributions for both u and d quarks. Building upon our previous study, we have extended the Fock-space truncation to include a dynamical gluon, thereby incorporating contributions from the q - g - q correlator—i.e., the genuine twist-3 component. The light-front wave functions used in the overlap representation are obtained by diagonalizing the proton light-front Hamiltonian constructed for the $|qqq\rangle$ and $|qqqq\rangle$ Fock sectors, supplemented with a three-dimensional confinement potential.

Our calculations indicate that the genuine twist-3 contribution, while relatively small, is nevertheless non-negligible; in certain cases, it even induces a sign opposite to that of the non-genuine component. Qualitatively, our results show good overall consistency with those of Ref. [59], except for the $x\tilde{E}_{2T}^d$ distribution and in the region of small x and small $-t$. In addition, we have examined several key twist-3-related quantities—including the quark OAM, the total quark contribution to the nucleon spin, and the quark spin-orbit correlation—and many of these are in reasonable agreement with predictions from other model studies [58, 87, 90, 91].

In future work, we plan to extend our analysis to twist-3 GPDs at nonzero skewness and, more broadly, to the twist-3 distributions of gluons and sea quarks. The nonzero-skewness sector is particularly important, as these twist-3 GPDs enter the twist-3 DVCS amplitudes [65] and will be probed in forthcoming measure-

ments at the EIC and EicC [92]. With continued development of the BLFQ framework, we expect to improve the precision of our calculations, address remaining discrepancies in sum-rule relations, and provide more reliable predictions relevant to understanding the proton spin puzzle.

ACKNOWLEDGMENTS

We thank Jiangshan Lan, Zhi Hu, Zhimin Zhu and Jiatong Wu for many helpful discussions and useful advises. C. M. is supported by new faculty start up funding the Institute of Modern Physics, Chinese Academy of Sciences, Grants No. E129952YR0. X. Z. is supported by the National Natural Science Foundation of China under Grant No.12375143, by new faculty startup funding by the Institute of Modern Physics, Chinese Academy of Sciences, by Key Research Program of Frontier Sciences, Chinese Academy of Sciences, Grant No. ZDBS-LY-7020, by the Natural Science Foundation of Gansu Province, China, Grant No. 20JR10RA067, by the Foundation for Key Talents of Gansu Province, by the Central Funds Guiding the Local Science and Technology Development of Gansu Province, Grant No. 22ZY1QA006, by international partnership program of the Chinese Academy of Sciences, Grant No. 016GJHZ2022103FN, by the Strategic Priority Research Program of the Chinese Academy of Sciences, Grant No. XDB34000000, and by National Key R&D Program of China, Grant No. 2023YFA1606903. J. P. V. is supported by the Department of Energy under Grant No. DE-SC0023692. A portion of the computational resources were also provided by Dongjiang Yuan Intelligent Computing Center.

Appendix A: Overlap representations for twist-3 GPDs

We will present the overlap representations of all zero-skewness twist-3 GPDs in the following. For convenience, the following notations are adopted,

$$[dx]_n = \prod_{i=1}^n \frac{dx_i d^2 \vec{k}_i}{(16\pi^3)^n} 16\pi^3 \delta \left(1 - \sum x_i \right) \times \delta^2 \left(\sum \vec{k}_i \right) \delta(x - x_1), \quad (A1)$$

where the subscript 1 denotes the struck quark, and $[\Gamma] = \bar{u}(p', \lambda') \Gamma u(p, \lambda)$ encapsulates the helicity combinations of the struck quark. Additionally, ψ_n^Λ signifies the LFWF $\psi_{i=1, \dots, n}^\Lambda(x_i, p_i, \lambda_i)$, with Λ representing the proton helicity and λ_i represents the quark helicity. The constraint for spectators $\delta_{\lambda_2}^{\lambda'_2} \delta_{\lambda_3}^{\lambda'_3} \delta_{\lambda_4}^{\lambda'_4}$ is implicitly assumed. In the overlap expressions, the symbol Δ refers to the two-dimensional complex representation, i.e., $\Delta = \Delta_1 + i\Delta_2$.

Each overlap representation is divided into three parts.

For the $|qqq\rangle$ sector, we have

$$\mathcal{F}_{\Gamma,\Lambda'\Lambda}^{qqq} = \int [dx]_3 \sum_{\lambda'_1, \lambda_1} \left(\frac{p_{1\perp}}{x_1} [\Gamma \gamma^+ \gamma^\perp] + \frac{p'_{1\perp}}{x_1} [\gamma^\perp \gamma^+ \Gamma] + \frac{m_q}{x_1} [\Gamma \gamma^+] + \frac{m_q}{x_1} [\gamma^+ \Gamma] \right) \psi_3^{\Lambda'*} \psi_3^\Lambda. \quad (\text{A2})$$

A similar expression applies to the $|qqqg\rangle$ sector,

$$\mathcal{F}_{\Gamma,\Lambda'\Lambda}^{qqqg} = \int [dx]_4 \sum_{\lambda'_1, \lambda_1} \left(\frac{p_{1\perp}}{x_1} [\Gamma \gamma^+ \gamma^\perp] + \frac{p'_{1\perp}}{x_1} [\gamma^\perp \gamma^+ \Gamma] + \frac{m_q}{x_1} [\Gamma \gamma^+] + \frac{m_q}{x_1} [\gamma^+ \Gamma] \right) \psi_4^{\Lambda'*} \psi_4^\Lambda. \quad (\text{A3})$$

Regarding the interference term gen , which incorporates the q - g - q interaction, we have

$$\mathcal{F}_{\Gamma,\Lambda'\Lambda}^{gen} = \int [dx]_4 \sum_{\lambda'_1, \lambda_1, \lambda_g} \frac{g_s}{\sqrt{x_g}} \left\{ \left(\frac{\epsilon^j}{x'_1} [\Gamma \gamma^+ \gamma^j] + \frac{\epsilon^j}{x_1} [\gamma^j \gamma^+ \Gamma] \right) \psi_3^{\Lambda'*} \psi_4^\Lambda + \left(\frac{\epsilon^{j*}}{x'_1} [\Gamma \gamma^+ \gamma^j] + \frac{\epsilon^{j*}}{x_1} [\Gamma \gamma^+ \gamma^j] \right) \psi_4^{\Lambda'*} \psi_3^\Lambda \right\}, \quad (\text{A4})$$

where ϵ^μ is the gluon polarization vector.

The total contribution is the sum of these three components,

$$\mathcal{F}_{\Gamma,\Lambda'\Lambda}^{total} = \mathcal{F}_{\Gamma,\Lambda'\Lambda}^{qqq} + \mathcal{F}_{\Gamma,\Lambda'\Lambda}^{qqqg} + \mathcal{F}_{\Gamma,\Lambda'\Lambda}^{gen}. \quad (\text{A5})$$

Using the expressions derived above, we can explicitly formulate the overlap representations for all twist-3 GPDs

$$H_2 = \frac{P^+}{M} \mathcal{F}_{1,\uparrow\uparrow}^{total}, \quad (\text{A6})$$

$$E_2 = \frac{2P^+}{\Delta^*} \mathcal{F}_{1,\uparrow\downarrow}^{total}, \quad (\text{A7})$$

$$\tilde{H}_2 = \frac{P^+}{M} \mathcal{F}_{\gamma_5,\uparrow\uparrow}^{total}, \quad (\text{A8})$$

$$\tilde{E}_2 = -\frac{2P^+}{\Delta^*} \mathcal{F}_{\gamma_5,\uparrow\downarrow}^{total}, \quad (\text{A9})$$

$$H_{2T}^j = \frac{(-i)^{(j-1)} P^+}{Mi(\Delta + (-)^j \Delta^*)} \left(\Delta \mathcal{F}_{\gamma^j,\uparrow\downarrow}^{total} + \Delta^* \mathcal{F}_{\gamma^j,\downarrow\downarrow}^{total} \right), \quad (\text{A10})$$

$$E_{2T}^j = \frac{P^+}{\Delta_j} \left(\mathcal{F}_{\gamma^j,\uparrow\uparrow}^{total} + \mathcal{F}_{\gamma^j,\downarrow\downarrow}^{total} \right) + \frac{2MP^+}{i^j \Delta_1 \Delta_2} \left(\mathcal{F}_{\gamma^j,\uparrow\downarrow}^{total} - (-)^j \mathcal{F}_{\gamma^j,\downarrow\uparrow}^{total} \right), \quad (\text{A11})$$

$$\tilde{H}_{2T}^j = -\frac{MP^+}{i^j \Delta_1 \Delta_2} \left(\mathcal{F}_{\gamma^j,\uparrow\downarrow}^{total} - (-)^j \mathcal{F}_{\gamma^j,\downarrow\uparrow}^{total} \right), \quad (\text{A12})$$

$$\tilde{E}_{2T}^j = \frac{2i^{(j-1)} P^+}{\Delta + (-)^j \Delta^*} \left(\mathcal{F}_{\gamma^j,\uparrow\uparrow}^{total} - \mathcal{F}_{\gamma^j,\downarrow\downarrow}^{total} \right), \quad (\text{A13})$$

$$H_{2T}^j = \frac{P^+}{2M\Delta_j} \left(\Delta \mathcal{F}_{\gamma^j,\gamma_5,\uparrow\downarrow}^{total} + \Delta^* \mathcal{F}_{\gamma^j,\gamma_5,\downarrow\uparrow}^{total} \right), \quad (\text{A14})$$

$$\begin{aligned} E_{2T}^j = & \frac{2i^{(j-1)} P^+}{\Delta + (-)^j \Delta^*} \left(\mathcal{F}_{\gamma^j,\gamma_5,\uparrow\uparrow}^{total} + \mathcal{F}_{\gamma^j,\gamma_5,\downarrow\downarrow}^{total} \right) \\ & + \frac{2MP^+}{i^{(2-j)} \Delta_1 \Delta_2} \left((-)^j \mathcal{F}_{\gamma^j,\gamma_5,\uparrow\downarrow}^{total} + \mathcal{F}_{\gamma^j,\gamma_5,\downarrow\uparrow}^{total} \right), \end{aligned} \quad (\text{A15})$$

$$H_{2T}^j = \frac{(-)^{(j-1)} MP^+}{i^{(2-j)} \Delta_1 \Delta_2} \left(\mathcal{F}_{\gamma^j,\gamma_5,\uparrow\downarrow}^{total} - (-)^j \mathcal{F}_{\gamma^j,\gamma_5,\downarrow\uparrow}^{total} \right), \quad (\text{A16})$$

$$\tilde{E}_{2T}^j = \frac{P^+}{\Delta_j} \left(\mathcal{F}_{\gamma^j,\gamma_5,\uparrow\uparrow}^{total} - \mathcal{F}_{\gamma^j,\gamma_5,\downarrow\downarrow}^{total} \right), \quad (\text{A17})$$

$$H_2' = \frac{iP^+}{M} \mathcal{F}_{i\sigma^{12},\gamma_5,\uparrow\uparrow}^{total}, \quad (\text{A18})$$

$$E_2' = \frac{2iP^+}{\Delta^*} \mathcal{F}_{i\sigma^{12},\gamma_5,\uparrow\downarrow}, \quad (\text{A19})$$

$$\tilde{H}_2' = \frac{P^+}{M} \mathcal{F}_{i\sigma^{+-},\gamma_5,\uparrow\uparrow}, \quad (\text{A20})$$

$$\tilde{E}_2' = -\frac{2P^+}{\Delta^*} \mathcal{F}_{i\sigma^{+-},\gamma_5,\uparrow\downarrow}, \quad (\text{A21})$$

where M denotes the proton mass. All the numerical results presented in this work are calculated using these overlap representations, and the LFWF obtained from the BLFQ framework.

Appendix B: Relations Between Different GPDs

The relations between GPDs defined in Ref. [80] and in [79] are

$$H_{2T} = 2\xi G_4, \quad (\text{B1})$$

$$E_{2T} = 2(G_3 - \xi G_4), \quad (\text{B2})$$

$$\tilde{H}_{2T} = \frac{1}{2} G_1, \quad (\text{B3})$$

$$\tilde{E}_{2T} = -(H + E + G_2) + 2(\xi G_3 - G_4), \quad (\text{B4})$$

$$H_{2T}' = \frac{-t}{4M^2} (\tilde{E} + \tilde{G}_1) + (\tilde{H} + \tilde{G}_2) - 2\xi \tilde{G}_3, \quad (\text{B5})$$

$$E_{2T}' = -(\tilde{E} + \tilde{G}_1) - (\tilde{H} + \tilde{G}_2) + 2(\xi \tilde{G}_3 - \tilde{G}_4), \quad (\text{B6})$$

$$\tilde{H}_{2T}' = \frac{1}{2} (\tilde{E} + \tilde{G}_1), \quad (\text{B7})$$

$$\tilde{E}_{2T}' = 2(\tilde{G}_3 - \xi \tilde{G}_4). \quad (\text{B8})$$

The inversion of above equations is

$$G_1 = 2\tilde{H}_{2T}, \quad (\text{B9})$$

$$G_2 = -(H + E) - \frac{1}{\xi} (1 - \xi^2) H_{2T} + \xi E_{2T} - \tilde{E}_{2T}, \quad (\text{B10})$$

$$G_3 = \frac{1}{2} (H_{2T} + E_{2T}), \quad (\text{B11})$$

$$G_4 = \frac{1}{2\xi} H_{2T}, \quad (\text{B12})$$

$$\tilde{G}_1 = -\tilde{E} + 2\tilde{H}'_{2T}, \quad (B13)$$

$$\tilde{G}_2 = -\tilde{H} + (1 - \xi^2)H'_{2T} - \xi^2 E'_{2T} - \frac{\Delta_\perp^2}{2M^2} \tilde{H}'_{2T} + \xi \tilde{E}'_{2T}, \quad (B14)$$

$$\tilde{G}_3 = -\frac{\xi}{2}(H'_{2T} + E'_{2T}) - \frac{\xi \bar{M}^2}{M^2} \tilde{H}'_{2T} + \frac{1}{2} \tilde{E}'_{2T}, \quad (B15)$$

$$\tilde{G}_4 = -\frac{1}{2}(H'_{2T} + E'_{2T}) - \frac{\bar{M}^2}{M^2} \tilde{H}'_{2T}, \quad (B16)$$

where $\bar{M}^2 = M^2 + t/4$.

The relations between GPDs defined in Ref. [81] and this work are

$$E_{2T}(x, \xi, -t) = 2G_{q,2}(x, \xi, -t), \quad (B17)$$

$$H_{2T}(x, \xi, -t) = G_{q,4}(x, \xi, -t), \quad (B18)$$

$$\tilde{E}_{2T}(x, \xi, -t) = 2\xi G_{q,2}(x, \xi, -t) - G_{q,3}(x, \xi, -t), \quad (B19)$$

$$\tilde{H}_{2T}(x, \xi, -t) = G_{q,1}(x, \xi, -t). \quad (B20)$$

[1] Stefan Diehl. Experimental exploration of the 3D nucleon structure. *Prog. Part. Nucl. Phys.*, 133:104069, 2023.

[2] Cédric Lorcé, Andreas Metz, Barbara Pasquini, and Peter Schweitzer. Parton Distribution Functions and their Generalizations. 7 2025.

[3] FX Girod, RA Niyazov, H Avakian, J Ball, I Bednitskiy, VD Burkert, R De Masi, L Elouadrhiri, M Garçon, M Guidal, et al. Measurement of deeply virtual compton scattering beam-spin asymmetries. *Physical review letters*, 100(16):162002, 2008.

[4] S Pisano, A Biselli, S Niccolai, E Seder, M Guidal, M Mirazita, KP Adhikari, D Adikaram, MJ Amaryan, MD Anderson, et al. Single and double spin asymmetries for deeply virtual compton scattering measured with clas and a longitudinally polarized proton target. *Physical Review D*, 91(5):052014, 2015.

[5] Hyon-Suk Jo, FX Girod, H Avakian, VD Burkert, M Garçon, M Guidal, V Kubarovský, S Niccolai, P Stoler, KP Adhikari, et al. Cross sections for the exclusive photon electroproduction on the proton and generalized parton distributions. *Physical review letters*, 115(21):212003, 2015.

[6] M Hattawy, NA Baltzell, R Dupré, S Bültmann, R De Vita, A El Alaoui, L El Fassi, H Egiyan, FX Girod, M Guidal, et al. Exploring the structure of the bound proton with deeply virtual compton scattering. *Physical Review Letters*, 123(3):032502, 2019.

[7] C Munoz Camacho, Alexandre Camsonne, Malek Mazouz, Catherine Ferdi, Gagik Gavalian, Elena Kuchina, M Amarian, KA Aniol, Matthieu Beaumel, Hachemi Benaoum, et al. Scaling tests of the cross section for deeply virtual compton scattering. *Physical review letters*, 97(26):262002, 2006.

[8] M Mazouz, A Camsonne, C Munoz Camacho, C Ferdi, G Gavalian, E Kuchina, M Amarian, KA Aniol, M Beaumel, H Benaoum, et al. Deeply virtual compton scattering off the neutron. *Physical review letters*, 99(24):242501, 2007.

[9] Catherine Adloff, V Andreev, B Andrieu, T Anthopoulos, V Arkadov, A Astvatsatourov, A Babaev, J Bähr, P Baranov, E Barrelet, et al. Measurement of deeply virtual compton scattering at hera. *Physics Letters B*, 517(1-2):47–58, 2001.

[10] Francise D Aaron, A Aktas, C Alexa, V Andreev, B Antunovic, S Aplin, A Asmone, A Astvatsatourov, S Backovic, A Baghdasaryan, et al. Measurement of deeply virtual compton scattering and its t-dependence at hera. *Physics Letters B*, 659(4):796–806, 2008.

[11] Francise D Aaron, M Aldaya Martin, C Alexa, K Almujiang, V Andreev, B Antunovic, S Backovic, A Baghdasaryan, E Barrelet, W Bartel, et al. Deeply virtual compton scattering and its beam charge asymmetry in e \pm p collisions at hera. *Physics Letters B*, 681(5):391–399, 2009.

[12] Zeus Collaboration et al. A measurement of the q₂, w and t dependences of deeply virtual compton scattering at hera. *Journal of High Energy Physics*, 2009(05):108, 2009.

[13] A Airapetian, N Akopov, Z Akopov, EC Aschenauer, W Augustyniak, R Avakian, A Avetissian, E Avetisyan, HP Blok, A Borissov, et al. Beam-helicity and beam-charge asymmetries associated with deeply virtual compton scattering on the unpolarised proton. *Journal of High Energy Physics*, 2012(7):1–26, 2012.

[14] A Airapetian, N Akopov, Z Akopov, EC Aschenauer, W Augustyniak, R Avakian, A Avetissian, E Avetisyan, S Belostotski, HP Blok, et al. Beam-helicity asymmetry arising from deeply virtual compton scattering measured with kinematically complete event reconstruction. *Journal of High Energy Physics*, 2012(10):1–28, 2012.

[15] R Abdul Khalek, A Accardi, J Adam, D Adamiak, W Akers, M Albaladejo, A Al-Bataineh, MG Alexeev, F Ameli, P Antonioli, et al. Science requirements and detector concepts for the electron-ion collider: Eic yellow report. *Nuclear Physics A*, 1026:122447, 2022.

[16] Daniele P Anderle, Valerio Bertone, Xu Cao, Lei Chang, Ningbo Chang, Gu Chen, Xurong Chen, Zhuojun Chen, Zhufang Cui, Lingyun Dai, et al. Electron-ion collider in china. *Frontiers of Physics*, 16:1–78, 2021.

[17] Xiang-Dong Ji, W. Melnitchouk, and X. Song. A Study of off forward parton distributions. *Phys. Rev. D*, 56:5511–5523, 1997.

[18] I. V. Anikin, D. Binosi, R. Medrano, S. Noguera, and V. Vento. Single spin asymmetry parameter from deeply virtual Compton scattering of hadrons up to twist - three accuracy. 1. Pion case. *Eur. Phys. J. A*, 14:95–103, 2002.

[19] K. Goeke, Maxim V. Polyakov, and M. Vanderhaeghen. Hard exclusive reactions and the structure of hadrons. *Prog. Part. Nucl. Phys.*, 47:401–515, 2001.

[20] V. Yu. Petrov, P. V. Pobylitsa, Maxim V. Polyakov, I. Bornig, K. Goeke, and C. Weiss. Off - forward quark distributions of the nucleon in the large N(c) limit. *Phys. Rev. D*, 57:4325–4333, 1998.

[21] M. Penttinen, Maxim V. Polyakov, and K. Goeke. Helicity skewed quark distributions of the nucleon and chiral symmetry. *Phys. Rev. D*, 62:014024, 2000.

[22] Sergio Scopetta and Vicente Vento. Generalized parton distributions and composite constituent quarks. *Phys.*

Rev. D, 69:094004, 2004.

[23] Sergio Scopetta and Vicente Vento. Generalized parton distributions in constituent quark models. *Eur. Phys. J. A*, 16:527–535, 2003.

[24] S. Boffi, B. Pasquini, and M. Traini. Linking generalized parton distributions to constituent quark models. *Nucl. Phys. B*, 649:243–262, 2003.

[25] S. Boffi, B. Pasquini, and M. Traini. Helicity dependent generalized parton distributions in constituent quark models. *Nucl. Phys. B*, 680:147–163, 2004.

[26] Sergio Scopetta and Vicente Vento. Helicity-dependent generalized parton distributions and composite constituent quarks. *Phys. Rev. D*, 71:014014, 2005.

[27] Chandan Mondal. Helicity-dependent generalized parton distributions for nonzero skewness. *Eur. Phys. J. C*, 77(9):640, 2017.

[28] Tanmay Maji, Chandan Mondal, and Dipankar Chakrabarti. Leading twist generalized parton distributions and spin densities in a proton. *Phys. Rev. D*, 96(1):013006, 2017.

[29] Dipankar Chakrabarti and Chandan Mondal. Chiral-odd generalized parton distributions for proton in a light-front quark-diquark model. *Phys. Rev. D*, 92(7):074012, 2015.

[30] Tanmay Maji, Chandan Mondal, D. Chakrabarti, and O. V. Teryaev. Relating transverse structure of various parton distributions. *JHEP*, 01:165, 2016.

[31] Chandan Mondal and Dipankar Chakrabarti. Generalized parton distributions and transverse densities in a light-front quark-diquark model for the nucleons. *Eur. Phys. J. C*, 75(6):261, 2015.

[32] B. Pasquini and S. Boffi. Virtual meson cloud of the nucleon and generalized parton distributions. *Phys. Rev. D*, 73:094001, 2006.

[33] B. Pasquini and S. Boffi. Generalized parton distributions in a meson cloud model. *Nucl. Phys. A*, 782:86–92, 2007.

[34] Alfredo Vega, Ivan Schmidt, Thomas Gutsche, and Valery E. Lyubovitskij. Generalized parton distributions in AdS/QCD. *Phys. Rev. D*, 83:036001, 2011.

[35] Dipankar Chakrabarti and Chandan Mondal. Generalized Parton Distributions for the Proton in AdS/QCD. *Phys. Rev. D*, 88(7):073006, 2013.

[36] Matteo Rinaldi. GPDs at non-zero skewness in ADS/QCD model. *Phys. Lett. B*, 771:563–567, 2017.

[37] Marco Claudio Traini. Generalized Parton Distributions: confining potential effects within AdS/QCD. *Eur. Phys. J. C*, 77(4):246, 2017.

[38] Guy F. de Teramond, Tianbo Liu, Raza Sabbir Sufian, Hans Günter Dosch, Stanley J. Brodsky, and Alexandre Deur. Universality of Generalized Parton Distributions in Light-Front Holographic QCD. *Phys. Rev. Lett.*, 120(18):182001, 2018.

[39] Bheemsehan Gurjar, Chandan Mondal, and Dipankar Chakrabarti. Polarized gluon distribution in the proton from holographic light-front QCD. *Phys. Rev. D*, 107(5):054013, 2023.

[40] B. C. Tiburzi and G. A. Miller. Exploring skewed parton distributions with two-body models on the light front. 1. Bimodality. *Phys. Rev. C*, 64:065204, 2001.

[41] B. C. Tiburzi and G. A. Miller. Exploring skewed parton distributions with two-body models on the light front 2: Covariant Bethe-Salpeter approach. *Phys. Rev. D*, 65:074009, 2002.

[42] A. Mukherjee and M. Vanderhaeghen. Helicity dependent twist two and twist three generalized parton distributions in light front QCD. *Phys. Rev. D*, 67:085020, 2003.

[43] Bolang Lin, Sreeraj Nair, Siqi Xu, Zhi Hu, Chandan Mondal, Xingbo Zhao, and James P. Vary. Generalized parton distributions of gluon in proton: A light-front quantization approach. *Phys. Lett. B*, 847:138305, 2023.

[44] Bolang Lin, Sreeraj Nair, Chandan Mondal, Siqi Xu, Zhi Hu, Pengxiang Zhang, Xingbo Zhao, and James P. Vary. Chiral-odd gluon generalized parton distributions in the proton: A light-front quantization approach. *Phys. Lett. B*, 860:139153, 2025.

[45] Ziqi Zhang, Zhi Hu, Siqi Xu, Chandan Mondal, Xingbo Zhao, James P Vary, and (BLFQ Collaboration). Twist-3 generalized parton distribution for the proton from basis light-front quantization. *Physical Review D*, 109(3):034031, 2024.

[46] Xiangdong Ji. Parton Physics on a Euclidean Lattice. *Phys. Rev. Lett.*, 110:262002, 2013.

[47] Xiangdong Ji, Yu-Sheng Liu, Yizhuang Liu, Jian-Hui Zhang, and Yong Zhao. Large-momentum effective theory. *Rev. Mod. Phys.*, 93(3):035005, 2021.

[48] Huey-Wen Lin. Nucleon helicity generalized parton distribution at physical pion mass from lattice QCD. *Phys. Lett. B*, 824:136821, 2022.

[49] Huey-Wen Lin. Nucleon Tomography and Generalized Parton Distribution at Physical Pion Mass from Lattice QCD. *Phys. Rev. Lett.*, 127(18):182001, 2021.

[50] Shohini Bhattacharya, Krzysztof Cichy, Martha Constantinou, Jack Dodson, Xiang Gao, Andreas Metz, Swagato Mukherjee, Aurora Scapellato, Fernanda Steffens, and Yong Zhao. Generalized parton distributions from lattice QCD with asymmetric momentum transfer: Unpolarized quarks. *Phys. Rev. D*, 106(11):114512, 2022.

[51] Constantia Alexandrou, Krzysztof Cichy, Martha Constantinou, Kyriakos Hadjyiannakou, Karl Jansen, Aurora Scapellato, and Fernanda Steffens. Transversity GPDs of the proton from lattice QCD. *Phys. Rev. D*, 105(3):034501, 2022.

[52] C. Alexandrou et al. Moments of the nucleon transverse quark spin densities using lattice QCD. *Phys. Rev. D*, 107(5):054504, 2023.

[53] Yuxun Guo, Xiangdong Ji, and Kyle Shiells. Generalized parton distributions through universal moment parameterization: zero skewness case. *JHEP*, 09:215, 2022.

[54] Constantia Alexandrou, Krzysztof Cichy, Martha Constantinou, Kyriakos Hadjyiannakou, Karl Jansen, Aurora Scapellato, and Fernanda Steffens. Unpolarized and helicity generalized parton distributions of the proton within lattice QCD. *Phys. Rev. Lett.*, 125(26):262001, 2020.

[55] M. Gockeler, Ph. Hagler, R. Horsley, D. Pleiter, Paul E. L. Rakow, A. Schafer, G. Schierholz, and J. M. Zanotti. Quark helicity flip generalized parton distributions from two-flavor lattice QCD. *Phys. Lett. B*, 627:113–123, 2005.

[56] M. Göckeler, Ph. Hägler, R. Horsley, Y. Nakamura, D. Pleiter, P. E. L. Rakow, A. Schäfer, G. Schierholz, H. Stüben, and J. M. Zanotti. Transverse spin structure of the nucleon from lattice QCD simulations. *Phys. Rev. Lett.*, 98:222001, 2007.

[57] C. Alexandrou et al. Moments of nucleon generalized parton distributions from lattice QCD simulations at physical pion mass. *Phys. Rev. D*, 101(3):034519, 2020.

[58] Chentao Tan and Zhun Lu. Chiral-even twist-3 gpds for the proton in a spectator diquark model. *Physical Review D*, 110(7):074027, 2024.

[59] Sameer Jain, Shubham Sharma, and Harleen Dahiya. Deciphering twist-3 chiral-even gpds in the light-front quark-diquark model. *Physical Review D*, 110(9):094030, 2024.

[60] Xiangdong Ji. Gauge-invariant decomposition of nucleon spin. *Physical Review Letters*, 78(4):610, 1997.

[61] Yoshitaka Hatta and Shinsuke Yoshida. Twist analysis of the nucleon spin in qcd. *Journal of high energy physics*, 2012(10):1–16, 2012.

[62] R.L. Jaffe and Aneesh Manohar. The g1 problem: Deep inelastic electron scattering and the spin of the proton. *Nuclear Physics B*, 337(3):509–546, 1990.

[63] Matthias Burkardt. Transverse force on quarks in deep-inelastic scattering. *Phys. Rev. D*, 88:114502, Dec 2013.

[64] Fatma P Aslan, Matthias Burkardt, and Marc Schlegel. Transverse force tomography. *Physical Review D*, 100(9):096021, 2019.

[65] Yuxun Guo, Xiangdong Ji, Brandon Kriesten, and Kyle Shiells. Twist-three cross-sections in deeply virtual compton scattering. *Journal of High Energy Physics*, 2022(6):1–48, 2022.

[66] J. P. Vary, H. Honkanen, Jun Li, P. Maris, S. J. Brodsky, A. Harindranath, G. F. de Teramond, P. Sternberg, E. G. Ng, and C. Yang. Hamiltonian light-front field theory in a basis function approach. *Phys. Rev. C*, 81:035205, 2010.

[67] N Kivel, Maxim V Polyakov, A Schäfer, and OV Teryaev. Wandzura-wilczek approximation for the twist-3 dvcs amplitude. *Physics Letters B*, 497(1-2):73–79, 2001.

[68] AV Radyushkin and C Weiss. Dvcs amplitude with kinematical twist-3 terms. *Physics Letters B*, 493(3-4):332–340, 2000.

[69] N Kivel and Maxim V Polyakov. Dvcs on the nucleon to the twist-3 accuracy. *Nuclear Physics B*, 600(2):334–350, 2001.

[70] AV Radyushkin and C Weiss. Kinematical twist-3 effects in deeply virtual compton scattering as a quark spin rotation. *Physical Review D*, 64(9):097504, 2001.

[71] Siqi Xu, Chandan Mondal, Xingbo Zhao, Yang Li, and James P. Vary. Quark and gluon spin and orbital angular momentum in the proton. *Phys. Rev. D*, 108(9):094002, 2023.

[72] Zhimin Zhu, Siqi Xu, Jiatong Wu, Hongyao Yu, Zhi Hu, Jiangshan Lan, Chandan Mondal, Xingbo Zhao, and James P. Vary. Transverse structure of the proton beyond leading twist: A light-front Hamiltonian approach. *Phys. Lett. B*, 855:138829, 2024.

[73] Sreeraj Nair, Chandan Mondal, Siqi Xu, Xingbo Zhao, James P Vary, BLFQ Collaboration, et al. Proton gravitational structure and mass decomposition on the light front. *Physical Review D*, 112(11):114001, 2025.

[74] Yang Li, Pieter Maris, Xingbo Zhao, and James P. Vary. Heavy Quarkonium in a Holographic Basis. *Phys. Lett. B*, 758:118–124, 2016.

[75] Xingbo Zhao, Heli Honkanen, Pieter Maris, James P. Vary, and Stanley J. Brodsky. Electron g-2 in Light-Front Quantization. *Phys. Lett. B*, 737:65–69, 2014.

[76] Hongyao Yu, Zhi Hu, Siqi Xu, Chandan Mondal, Xingbo Zhao, and James P. Vary. Transverse-momentum-dependent gluon distributions of proton within basis light-front quantization. *Phys. Lett. B*, 855:138831, 2024.

[77] Pengxiang Zhang, Yiping Liu, Siqi Xu, Chandan Mondal, Xingbo Zhao, and James P. Vary. Gluon skewed generalized parton distributions of proton from a light-front Hamiltonian approach. *Phys. Lett. B*, 866:139584, 2025.

[78] John B Kogut and Davison E Soper. Quantum electrodynamics in the infinite-momentum frame. *Physical Review D*, 1(10):2901, 1970.

[79] Stephan Meißner, Andreas Metz, and Marc Schlegel. Generalized parton correlation functions for a spin-1/2 hadron. *Journal of High Energy Physics*, 2009(08):056, 2009.

[80] Fatma Aslan, Matthias Burkardt, Cédric Lorcé, Andreas Metz, and Barbara Pasquini. Twist-3 generalized parton distributions in deeply-virtual compton scattering. *Phys. Rev. D*, 98:014038, Jul 2018.

[81] Yuxun Guo, Xiangdong Ji, and Kyle Shiells. Novel twist-three transverse-spin sum rule for the proton and related generalized parton distributions. *Nuclear Physics B*, 969:115440, 2021.

[82] Andrei V Belitsky, A Kirchner, Dieter Mueller, and A Schäfer. Twist-three observables in deeply virtual compton scattering on the nucleon. *Physics Letters B*, 510(1-4):117–124, 2001.

[83] Andrei V Belitsky, Dieter Mueller, and A Kirchner. Theory of deeply virtual compton scattering on the nucleon. *Nuclear Physics B*, 629(1-3):323–392, 2002.

[84] Xiangdong Ji, Xiaonu Xiong, and Feng Yuan. Probing parton orbital angular momentum in longitudinally polarized nucleon. *Phys. Rev. D*, 88:014041, Jul 2013.

[85] Fatma P. Aslan, Matthias Burkardt, and Marc Schlegel. Transverse force tomography. *Phys. Rev. D*, 100:096021, Nov 2019.

[86] DV Kiptily and MV Polyakov. Genuine twist-3 contributions to the generalized parton distributions from instantons. *The European Physical Journal C-Particles and Fields*, 37(1):105–114, 2004.

[87] Cédric Lorcé. Spin-orbit correlations in the nucleon. *Physics Letters B*, 735:344–348, 2014.

[88] Hugh Burkhardt and WN Cottingham. Sum rules for forward virtual compton scattering. *Annals of Physics*, 56(2):453–463, 1970.

[89] Cedric Lorcé and Barbara Pasquini. Quark wigner distributions and orbital angular momentum. *Physical Review D—Particles, Fields, Gravitation, and Cosmology*, 84(1):014015, 2011.

[90] Elliot Leader, Aleksander V Sidorov, and Dimiter B Stamenov. Determination of polarized parton densities from a qcd analysis of inclusive? format?; and semi-inclusive deep inelastic scattering data. *Physical Review D—Particles, Fields, Gravitation, and Cosmology*, 82(11):114018, 2010.

[91] Cédric Lorcé. Wilson lines and orbital angular momentum. *Physics Letters B*, 719(1-3):185–190, 2013.

[92] José Manuel Morgado Chávez, Valerio Bertone, Feliciano De Soto Borrero, Maxime Defurne, Cédric Mezrag, Hervé Moutarde, José Rodríguez-Quintero, and Jorge Segovia. Accessing the pion 3d structure at us and china electron-ion colliders. *Physical Review Letters*, 128(20):202501, 2022.